CHAPTER 4.

Drought Patterns in the Conterminous United States and Hawaii

Frank H. Koch
William D. Smith
John W. Coulston

INTRODUCTION

Droughts are common in virtually all U.S. forests, but their frequency and intensity vary widely both between and within forest ecosystems (Hanson and Weltzin 2000). Forests in the Western United States generally exhibit a pattern of annual seasonal droughts. Forests in the Eastern United States tend to exhibit one of two prevailing patterns: random occasional droughts, typical of the Appalachian Mountains and of the Northeast, or frequent late-summer droughts, typical of the southeastern Coastal Plain and the eastern edge of the Great Plains (Hanson and Weltzin 2000). For plants, a reduction in basic growth processes (i.e., cell division and enlargement) is the most immediate response to drought; photosynthesis, which is less sensitive than these basic processes, decreases slowly at low levels of drought stress but begins to decrease more sharply when the stress becomes moderate to severe (Kareiva and others 1993, Mattson and Haack 1987). Drought makes some forests more susceptible to infestations of tree-damaging insects and diseases (Clinton and others 1993, Mattson and Haack 1987). Furthermore, drought may increase wildland fire risk by impeding decomposition of organic matter and reducing the moisture content of downed woody materials and other potential fire fuels (Clark 1989, Keetch and Byram 1968, Schoennagel and others 2004).

Notably, forests appear to be relatively resistant to short-term drought conditions (Archaux and Wolters 2006), although individual tree species differ in their responses (Hinckley and others 1979, McDowell and others 2008). The duration of a drought event is arguably more significant than its intensity (Archaux and Wolters 2006); for example, multiple consecutive years of drought (2 to 5 years) are more likely to result in high tree mortality than a single dry year (Guarín and Taylor 2005, Millar and others 2007). This suggests that a comprehensive characterization of drought impact in forested areas should include analysis of moisture conditions in the United States during relatively long (i.e., multiyear) time windows.

In the Forest Health Monitoring (FHM) 2010 national report, we outlined a new methodology for mapping drought conditions across the conterminous United States (Koch and others 2013a). As in previous work related to this topic (Koch and others 2012a, 2012b), a primary objective of this new methodology was to provide forest managers and researchers with drought-related spatial datasets that are finer scale than products available from such sources as the National Climatic Data Center (2007) or the U.S. Drought Monitor Program (Svoboda and others 2002). The primary inputs are gridded climate data (i.e., monthly raster maps of precipitation and temperature over a 100-year period) created with the Parameter-Elevation

Regression on Independent Slopes (PRISM) climate mapping system (Daly and others 2002). A pivotal aspect of our new methodology is a standardized drought indexing approach that enables us to directly compare, for any given location of interest, its moisture status during different time windows, regardless of their length. For example, the FHM 2010 national report includes a comparison of national drought maps for 2009, the 3-year window 2007–09, and the 5-year window 2005–09 (Koch and others 2013a).

One of our main goals for the present analysis was to apply this methodology to the most currently available climate data (i.e., the monthly PRISM data through 2011). In turn, our results are intended to complement the results of similar analyses performed for the 2010 and 2011 FHM national reports, which were based on PRISM data through 2009 and 2010, respectively (Koch and others 2013a, 2013b). Thus, the current analysis represents a third time step in what we expect to be an ongoing annual record of drought status across the conterminous United States. In addition, we performed a separate analysis of drought patterns in Hawaii. Briefly, we developed 1-, 3-, and 5-year drought map products as data support for insect and disease risk mapping efforts in the State. However, unlike for the conterminous United States, we did not have monthly gridded climate data (i.e., PRISM data) of Hawaii as a foundation for our analysis. Therefore, we generated these grids ourselves through spatial interpolation of weather station observations recorded in Hawaii during an 88-year (1920-2007) period. Details about the interpolation process are provided in this chapter, along with a discussion of some highlights of our analytical results for the State.

METHODS

We acquired monthly PRISM grids for total precipitation, mean daily minimum temperature, and mean daily maximum temperature for the conterminous United States from the PRISM group Web site (PRISM Group 2012). When we performed our analyses, gridded datasets were available for all years from 1895 to 2011. However, the grids for May through December 2011 were only provisional versions (i.e., the PRISM group had not yet released finalized grids for these months). For the current analyses, we treated these provisional grids as if they were the final versions. The spatial resolution of the grids was approximately 4 km (cell area = 16 km^2); for future applications and to ensure better compatibility with other spatial datasets, all output grids were resampled to a spatial resolution of approximately 2 km (cell area = 4 km^2) using a nearest neighbor approach.

Potential Evapotranspiration Maps

As in our previous drought mapping efforts (Koch and others 2012a, 2012b, 2013a, 2013b), we adopted an approach in which a moisture index value for each location of interest (i.e., each grid cell in a map of the conterminous United States) was calculated based on both precipitation and potential evapotranspiration (*PET*) values for that location during the period of interest. *PET* measures the loss of soil moisture through plant uptake and transpiration (Akin 1991). It does not measure actual moisture loss, but rather the loss that would occur under ideal conditions (i.e., if there was no possible shortage of moisture for plants to transpire) (Akin 1991, Thornthwaite 1948). The ratio between precipitation and *PET* subsequently provides a fuller accounting of a location's water balance than precipitation alone.

To complement the available PRISM monthly precipitation grids, we computed corresponding monthly *PET* grids using Thornthwaite's formula (Akin 1991, Thornthwaite 1948):

$$PET_m = 1.6 L_{lm} \left(10 \frac{T_m}{I}\right)^a \qquad (1)$$

where

PET_m = the potential evapotranspiration for a given month m in cm

L_{lm} = a correction factor for the mean possible duration of sunlight during month m for all locations (i.e., grid cells) at a particular latitude l [see table V in Thornthwaite (1948) for a list of L correction factors by month and latitude]

T_m = the mean temperature for month m in degrees C

a = an exponent calculated as $a = 6.75 \times 10^{-7} I^3 - 7.71 \times 10^{-5} I^2 + 1.792 \times 10^{-2} I + 0.49239$ [see appendix I in Thornthwaite (1948) regarding the empirical derivation of a]

I = an annual heat index, calculated as $I = \sum_{m=1}^{12} \left(\frac{T_m}{5}\right)^{1.514}$ where

T_m = the mean temperature for each month m of the year

To implement equation 1 spatially, we created a grid of latitude values for determining the L adjustment for any given grid cell (and any given month) in the conterminous United States. We calculated the mean monthly temperature grids as the mean of the corresponding PRISM daily minimum and maximum monthly temperature grids.

Moisture Index Maps

We used the precipitation (*P*) and *PET* grids to generate baseline moisture index grids for the past 100 years (i.e., 1912–2011) for the conterminous United States. We used a moisture index, *MI′*, described by Willmott and Feddema (1992), with the following form:

$$MI' = \begin{cases} P/PET - 1 & , \quad P < PET \\ 1 - PET/P & , \quad P \geq PET \\ 0 & , \quad P = PET = 0 \end{cases} \qquad (2)$$

where

P = precipitation

PET = potential evapotranspiration

(*P* and *PET* must be in equivalent measurement units, e.g., mm)

This set of equations yields a dimensionless index scaled between -1 and 1. A key reason for using this particular equation set is that it ensures that *MI′* is centered at zero, with values below zero indicating moisture deficit and values greater than zero indicating moisture surplus. *MI′* can be calculated for any period but is commonly calculated on an annual basis using summed *P* and *PET* values (Willmott and Feddema 1992). An alternative to this summation approach is to calculate *MI′* from monthly *P* and *PET* values and then, for a given time window of interest, calculate its moisture index as the mean of the *MI′* values for all months in the window. This "mean-of-months" approach limits the ability of short-term peaks in either *P* or *PET* to negate corresponding short-term deficits, as would happen under a summation approach.

For each year in our study period (i.e., 1912–2011), we used the mean-of-months approach to calculate moisture index grids for three different time windows: 1 year (MI_1'), 3 years (MI_3'), 5 years (MI_5'). Briefly, the MI_1' grids are the mean of the 12 monthly *MI′* grids for each year in the study period, the MI_3' grids are the mean of the 36 monthly grids from January 2 years prior through December of the target year, and the MI_5' grids are the mean of the 60 consecutive monthly *MI′* grids from January 4 years prior to December of the target year. For example, for the year 2011, the MI_1' grid is the mean of the monthly *MI′* grids from January to December 2011, the MI_3' grid is the mean of grids from January 2009 to December 2011, and the MI_5' grid is the mean of the grids from January 2007 to December 2011.

Annual and Multiyear Drought Maps

To determine degree of departure from typical moisture conditions, we first created a normal grid, $MI_{i\,norm}'$ for each of our three time windows, representing the mean of the 100 corresponding moisture index grids (i.e., the MI_1', MI_3', or MI_5' grids, depending on the window; see fig. 4.1). We also created a standard deviation grid, $MI_{i\,SD}'$, for each time window, calculated from the window's 100 individual moisture index grids as well as its $MI_{i\,norm}'$ grid.

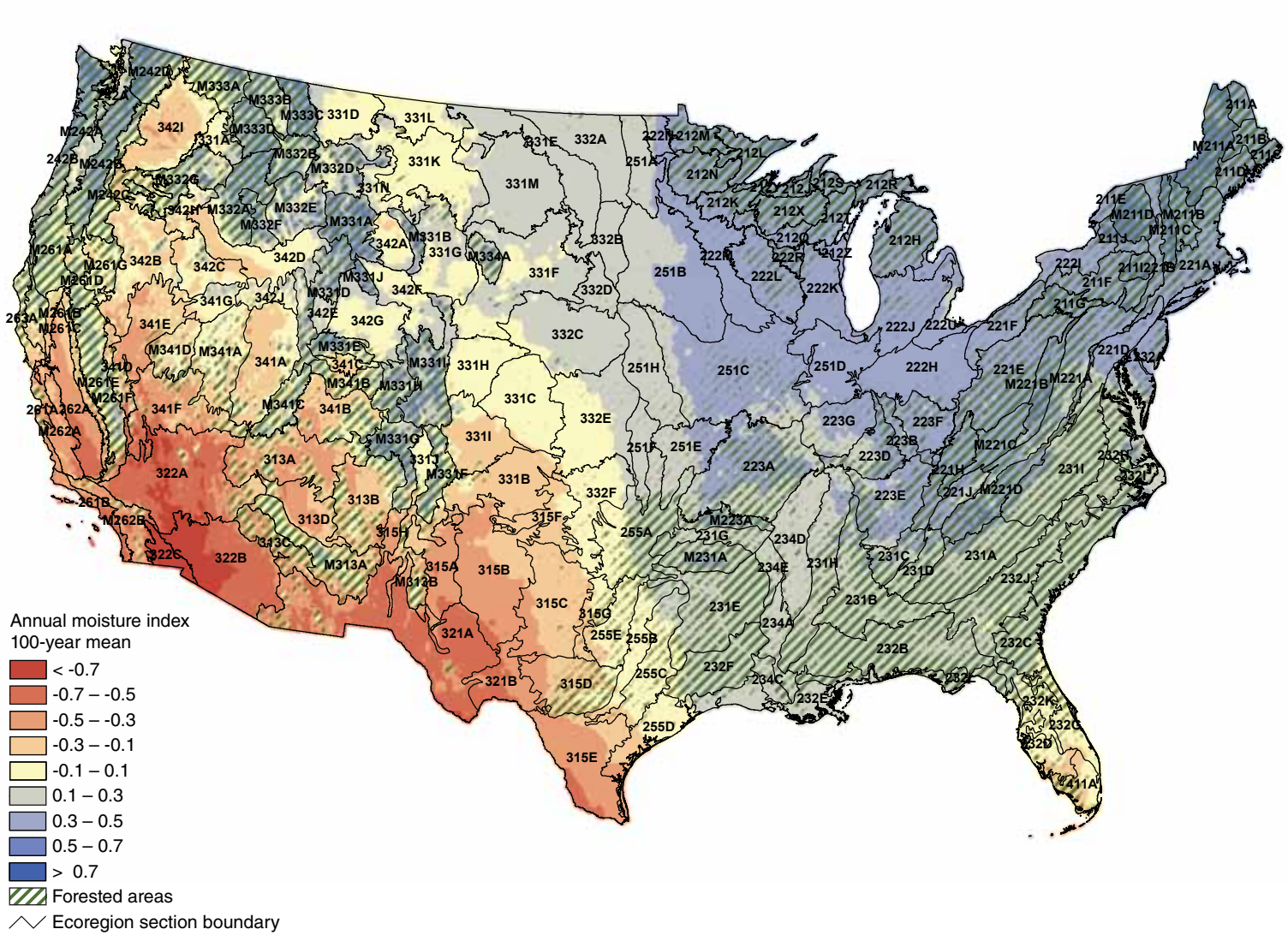

Figure 4.1—The 100-year (1912–2011) mean annual moisture index, or $\mathrm{MI}_1{}'_{\mathrm{norm}}$ *for the conterminous United States. Ecoregion section (Cleland and others 2007) boundaries and labels are included for reference. Forest cover data (overlaid green hatching) is derived from MODIS imagery by the USDA Forest Service Remote Sensing Applications Center. (Data source: PRISM Group, Oregon State University.)*

We subsequently calculated moisture difference *z*-scores (*MDZ*s) for each time window using these derived datasets:

$$MDZ_{ij} = \frac{MI_i' - MI_{i\ norm}'}{MI_{i\ SD}'} \qquad (3)$$

where

i = the analytical time window (1, 3, or 5 years)

j = a particular target year in our 100-year study period (i.e., 1911-2011)

*MDZ*s may be classified in terms of degree of moisture deficit or surplus (table 4.1). The classification scheme includes categories (e.g., severe drought or extreme drought) like those associated with the Palmer Drought Severity Index (Palmer 1965). Importantly, because of the standardization in equation 3, the breakpoints between categories remain the same regardless of the size of the time window of interest. For comparative analysis, we generated classified *MDZ* maps of the conterminous United States, based on all three time windows, for the target year 2011 (figs. 4.2, 4.3, and 4.4). Because our analysis focused on drought (i.e., moisture deficit) rather than surplus conditions, we combined the four moisture surplus categories from table 4.1 into a single category for map display.

Table 4.1—Moisture difference *z*-score (*MDZ*) value ranges for nine wetness and drought categories, along with each category's approximate theoretical frequency of occurrence

MDZ score value range	Category	Frequency
		%
< -2	Extreme drought	2.3
-2 to -1.5	Severe drought	4.4
-1.5 to -1	Moderate drought	9.2
-1 to -0.5	Mild drought	15.0
-0.5 to 0.5	Near-normal conditions	38.2
0.5 to 1	Mild moisture surplus	15.0
1 to 1.5	Moderate moisture surplus	9.2
1.5 to 2	Severe moisture surplus	4.4
> 2	Extreme moisture surplus	2.3

Drought map products for Hawaii

Because a historical record of monthly gridded climate data was unavailable for Hawaii, we generated monthly grids of total precipitation and average temperature through spatial interpolation of observations at weather stations distributed across the State. Several well-documented spatial interpolation methods include inverse distance weighting, spline, and the geostatistical procedure known as "kriging." All these methods similarly predict values for a variable of interest at unsampled locations based on the values recorded at nearby known locations. Kriging, in particular, makes its predictions by exploiting the underlying spatial structure of the variable, i.e., the spatial dependence or autocorrelation between

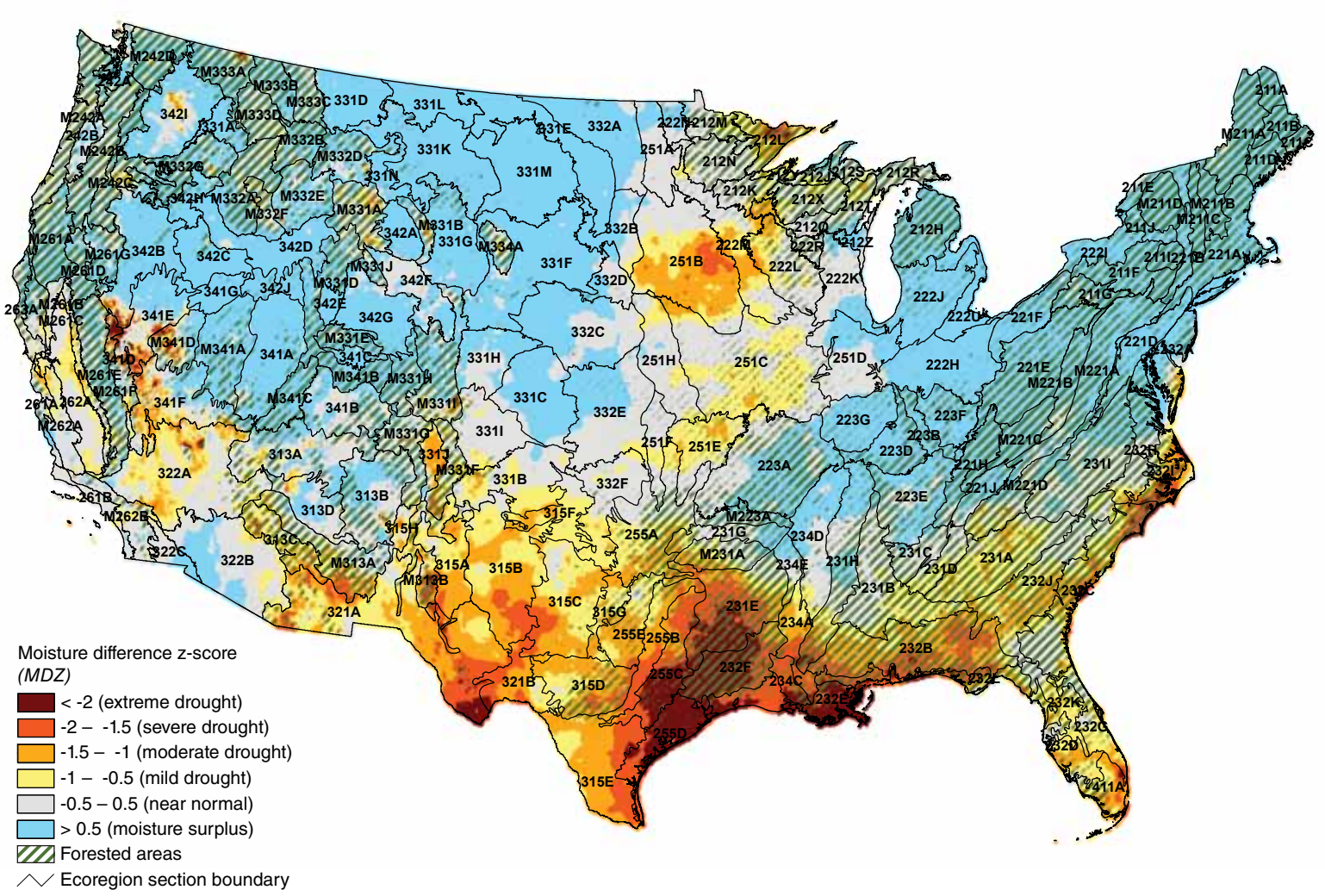

Figure 4.2—The 2011 annual (i.e., 1-year) moisture difference z-score, or MDZ, *for the conterminous United States. Ecoregion section (Cleland and others 2007) boundaries and labels are included for reference. Forest cover data (overlaid green hatching) is derived from MODIS imagery by the USDA Forest Service Remote Sensing Applications Center. (Data source: PRISM Group, Oregon State University.)*

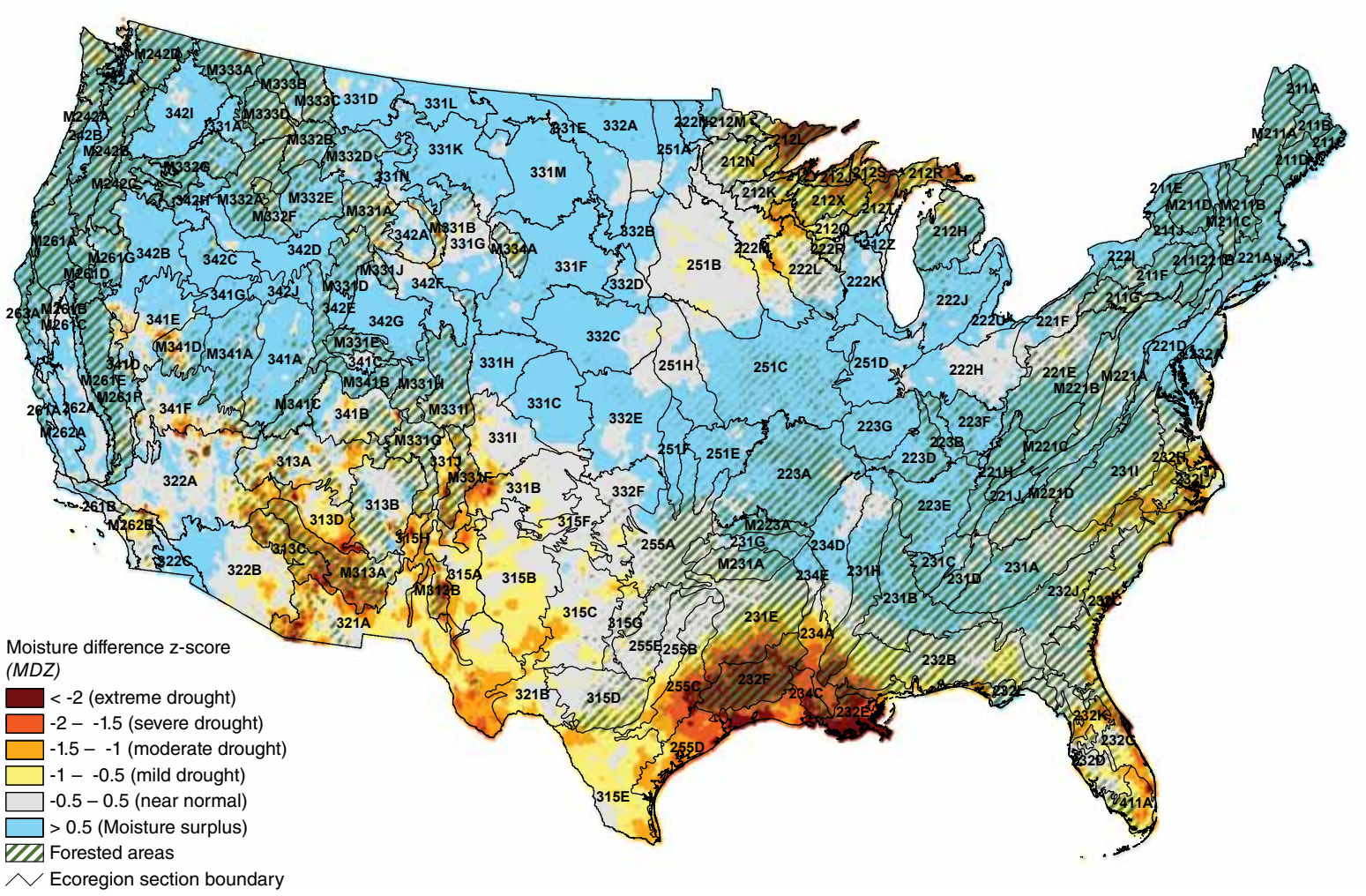

Figure 4.3—The 2009–11 (i.e., 3-year) moisture difference z-score, *or* MDZ, *for the conterminous United States. Ecoregion section (Cleland and others 2007) boundaries are included for reference. Forest cover data (overlaid green hatching) is derived from MODIS imagery by the USDA Forest Service Remote Sensing Applications Center. (Data source: PRISM Group, Oregon State University.)*

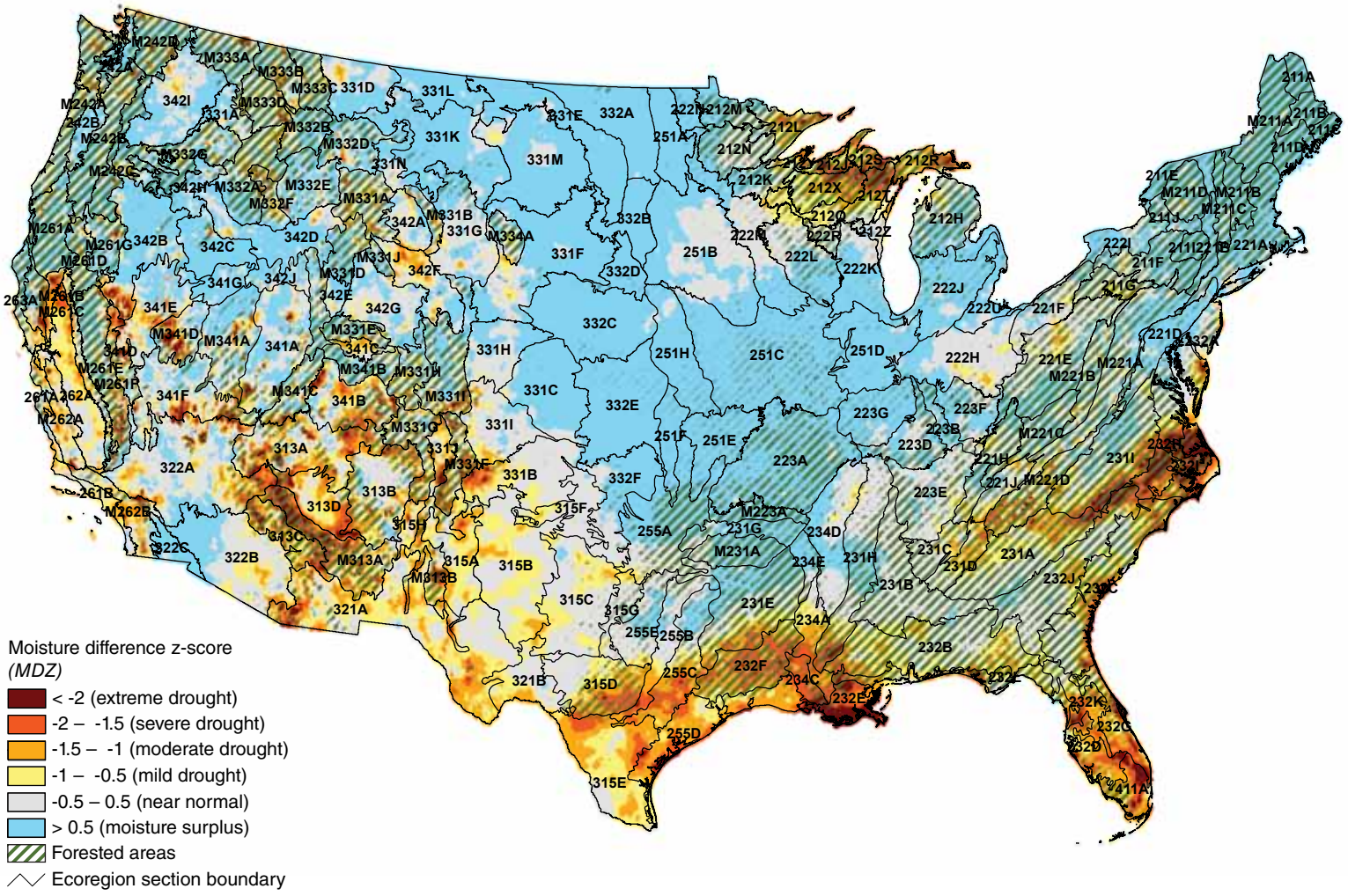

Figure 4.4—The 2007–11 (i.e., 5-year) moisture difference z-score, *or* MDZ, *for the conterminous United States. Ecoregion section (Cleland and others 2007) boundaries are included for reference. Forest cover data (overlaid green hatching) is derived from MODIS imagery by the USDA Forest Service Remote Sensing Applications Center. (Data source: PRISM Group, Oregon State University.)*

neighboring locations (Goovaerts 2000). This structure may be quantified using an empirical semivariogram constructed from pairs of known locations that comprise a sample of the variable (Cressie 1993). A model semivariogram (e.g., a spherical or exponential model) is fitted to the empirical semivariogram, which is then used to calculate "kriging weights" that are applied to a set of nearby known points in order to estimate the value at an unsampled location (Phillips and others 1992).

Cokriging is a multivariate version of kriging; the values for a variable of interest at unsampled locations are still estimated from neighboring known locations but, in this case, using values of one or more covariates as well as the variable of interest. This requires quantification of the spatial structure of each covariate (commonly done using additional semivariograms) as well the variables' cross-correlations or cross-covariance (Phillips and others 1992). Although this adds computational complexity, cokriging is especially suited to cases in which the target variable has been only sparsely sampled in space but a highly correlated covariate (or covariates) has been sampled more intensively. Elevation, which is often densely and regularly sampled, is a common covariate. For instance, elevation data have been used in cokriging of both precipitation (Hevesi and others 1992) and air temperature (Ishida and Kawashima 1993) from relatively sparse networks of observations. We applied ordinary cokriging (Cressie 1993, Goovaerts 1998), using elevation values drawn from a digital elevation model (DEM), to construct monthly grids of total precipitation and mean temperature for Hawaii.

Our source for precipitation data was *The Rainfall Atlas of Hawai'i* (Giambelluca and others 2011), which provided regular sets of rain gauge observations for each month from January 1920 until December 2007. The atlas assembled these data from a variety of sources, including the Office of the State Climatologist, the U.S. National Climatic Data Center (NCDC), the U.S. Geological Survey (USGS), and a variety of smaller rain gauge networks. Furthermore, because the rain gauges in these networks had different periods of operation, the researchers who constructed the atlas dataset employed a process of "gap-filling" (i.e., statistically estimating precipitation values for rain gauges that were not operational at a particular point in time) in order to improve spatial coverage. As a result, we were able to perform our interpolations based on more than 1,000 precipitation observations in any given month and year. These observations were distributed across all of the major Hawaiian Islands except Ni'ihau, which was therefore omitted from our analyses.

We acquired monthly mean temperature data for Hawaii from the NCDC (National Climatic Data Center 2012a). Over the period of interest (January 1920 to December 2007), the average number of temperature observations available each month was 46 (minimum = 28, maximum = 69). Although there were considerably more

observations of precipitation than temperature in any given month, temperature is less spatially variable (Gómez and others 2008) and so may be interpolated more reliably from fewer data. Regarding elevation, the USGS had previously developed a 30-m resolution DEM for Hawaii. To reduce computation time, however, we resampled the original DEM to a resolution of 240 m (using the cubic convolution method). We used this resampled DEM in all of our interpolations.

We performed cokriging of precipitation and temperature separately for each month of the study period. We set up the interpolations for each variable as batch processes, which we executed using the Geostatistical Analyst extension of the ArcGIS software package (ESRI 2010). Each month, all model semivariogram (i.e., the stable semivariogram model; see Johnston and others 2003) parameters for elevation and the target variable, as well as the cross-covariance, were automatically refitted using the weighted least squares approach (Cressie 1993). Before calculating these parameters, we removed either a first-order (temperature) or second-order (precipitation) trend from the climate data to minimize macroscale variation. We did not detrend the elevation data. After calculating the semivariograms and cross-covariance, we used circular search windows (with the optimal radial distance recalculated each month) to define neighborhoods of sampled locations used in predicting values at unsampled locations. In summary, predicted values were based on from 2 to 5 observations of the target variable (i.e., either temperature or precipitation) and up to 20 elevation observations. (Trials with different neighborhoods revealed only minor changes in prediction estimates.) The output interpolated grids had a spatial resolution of 2 km (cell area = 4 km^2).

After completing the cokriging operations, we used the interpolated grids to develop drought-related map products for Hawaii in a manner similar to our procedure for the conterminous United States. First, we used the temperature grids to develop *PET* grids for each month in our study period (see equation 1). Next, we applied the monthly *PET* grids and corresponding *P* grids to develop baseline moisture index grids for the 1-year, 3-year, and 5-year time windows (i.e., MI_1', MI_3', and MI_5' grids; see equation 2). From these moisture index grids, we calculated $MI_{i\,norm}'$ and $MI_{i\,SD}'$ grids for each time window, which we then used to create a full set of classified *MDZ* maps for the study period (see equation 3). The only noteworthy difference between our analyses for the conterminous United States and Hawaii is that we had a total of 88 years (i.e., 1920–2007) of available data for the latter, as opposed to more than 110 years for the former. This meant that we had to calculate the $MI_{1\,norm}'$ and $MI_{1\,SD}'$ grids for Hawaii (and the corresponding *MDZ* maps) based on an 88-year window. Moreover, because we did not have additional years of data before 1920, we were limited to an 86-year (1922–2007) window

for $MI_{3\,norm}'$, $MI_{3\,SD}'$, and the corresponding *MDZ* maps, as well as an 84-year (1924–2007) window for $MI_{5\,norm}'$, $MI_{3\,SD}'$, and their corresponding maps.

To investigate long-term drought patterns in Hawaii, we created a series of four drought frequency grids by overlaying the annual (i.e., 1-year) *MDZ* maps and subsequently calculating, for each map cell, the proportion of years out of 88 that the cell exhibited the following conditions: at least mild drought (*MDZ* < -0.5), at least moderate drought (*MDZ* < -1), at least severe drought (*MDZ* < -1.5), and extreme drought (*MDZ* < -2). We adopted a similar approach for the 3- and 5-year drought windows. Briefly, we overlaid the appropriate set of *MDZ* grids and counted the number of times (out of 86 and 84, respectively) in which grid cell values indicated at least mild, at least moderate, at least severe, or extreme drought conditions. We then divided these counts by the matching value (i.e., 86 or 84) to estimate 3- and 5-year drought frequencies in the outlined drought categories.

RESULTS AND DISCUSSION

Conterminous United States

The 100-year (1912–2011) mean annual moisture index, or $MI_{1\,norm}'$, grid (fig. 4.1) provides a relatively long-term historical overview of climatic regimes across the conterminous United States. (Because the 100-year $MI_{3\,norm}'$ and $MI_{5\,norm}'$ grids were very similar to the mean $MI_{1\,norm}'$ grid, they are not shown here.) Wet climates ($MI' > 0$) are typical throughout the Eastern United States, especially the Northeast. Southern Florida—in particular ecoregion sections 232C-Florida Coastal Lowlands-Atlantic, 232D-Florida Coastal Lowlands-Gulf, and 411A-Everglades—appears to be, perhaps surprisingly, the driest region of the Eastern United States. Although this region usually receives a high level of *P*, this is counteracted by a high level of *PET*, resulting in negative *MI*′ values. The apparent dryness of southern Florida (i.e., where high *P* is offset by high *PET*) arises from very different circumstances than those observed in the driest parts of the Western United States, especially the Southwest (e.g., sections 322A-Mojave Desert, 322B-Sonoran Desert, and 322C-Colorado Desert), where *PET* is very high but *P* levels are very low. In fact, dry climates ($MI' < 0$) are common across much of the Western United States because of generally lower precipitation than in the East. Yet, mountainous areas in the central and northern Rocky Mountains and in the Pacific Northwest are relatively wet; for example, ecoregion sections M242A-Oregon and Washington Coast Ranges, M242B-Western Cascades, M331G-South-Central Highlands, and M333C-Northern Rockies. This may be partially shaped by high levels of winter snowfall in these regions.

Figure 4.2 shows the annual (i.e., 1-year) *MDZ* map for 2011 for the conterminous United States. Its most distinctive feature is a nearly continuous swath of moderate-to-extreme drought conditions stretching across the southern portion of the country.

The western end of this swath is essentially defined by a cluster of areas with extreme drought (*MDZ* < -2) conditions in ecoregion sections 341D-Mono, 341E-Northern Mono, and M341D-West Great Basin and Mountains; however, only in the latter section do these conditions appear to affect forested areas. The eastern end of the swath is demarcated by an area of moderate to extreme drought along the southeast Atlantic coast, especially in the northern portion of ecoregion section 232C-Atlantic Coastal Flatwoods and the adjacent portion of section 232I-Northern Atlantic Coastal Flatwoods.

The swath includes three sizeable and contiguous "hot spots" of extreme drought. The largest of these hot spots encompasses much of ecoregion sections 231E-Mid Coastal Plains-Western, 232F-Coastal Plains and Flatwoods-Western Gulf, 255C-Oak Woods and Prairie, and the sparsely forested section 255D-Central Gulf Prairie and Marshes. The second largest hot spot includes most of the eastern portion of section 232E-Louisiana Coastal Prairie and Marshes, but it also extends into two more heavily forested sections, 234C-Atchafalaya and Red River Alluvial Plains and 232L-Gulf Coastal Lowlands. Finally, another hot spot occupies the southeastern tip of section 321A-Chihuahuan Desert Basin and Range and extends into the adjacent section 321B-Stockton Plateau. (The area in question is largely unforested.) Taken together, these three hot spots—along with neighboring areas of moderate to severe drought—comprise an expansive region of intense drought conditions that spans the States of Texas and Louisiana. Both States, especially Texas, had historically dry years in 2011. Furthermore, both States experienced record heat during the summer months (National Climatic Data Center 2012b).

North of this swath, most of the United States experienced a moisture surplus in 2011. In the Northeastern United States, there were isolated occurrences of mild drought, but the droughts were extremely limited in extent (i.e., encompassing no more than a few adjacent map cells). The northern Rocky Mountain and Pacific Northwest regions contained some larger pockets of moderate to extreme drought, perhaps most notably in the forested ecoregion sections M331A-Yellowstone Highlands and M333A-Okanogan Highland as well as the largely unforested section 342I-Columbia Basin. These examples notwithstanding, the northern Rockies and Pacific Northwest had precipitation levels far above normal through the first half of 2011, which offset drier-than-normal conditions in some portions of these regions during the latter half of the year (National Climatic Data Center 2012b).

A fairly extensive area of moderate to severe drought was centered on (largely unforested) section 251B-North Central Glaciated Plains. To the north of this area, in the heavily forested western Great Lakes region, there was a pronounced drought hot spot (moderate to extreme drought) in section 212L-Northern Superior Uplands. This represents a departure from 2010, when this region experienced record dryness (National Climatic Data Center 2011)

and many other nearby ecoregion sections (e.g., 212S-Northern Upper Peninsula) also exhibited extreme drought conditions.

Whereas the single-year *MDZ* map in figure 4.2 represents the most recent annual snapshot of moisture conditions across the conterminous United States, the 3-year (fig. 4.3) and 5-year (fig. 4.4) *MDZ* maps depict recent short-term trends in these conditions. For instance, the Southwestern United States has been regularly subject to intense and widespread droughts during the past two decades (Groisman and Knight 2008; Mueller and others 2005; National Climatic Data Center 2010, 2011; O'Driscoll 2007). The persistence of these conditions is partially illustrated by the 3-year and 5-year *MDZ* maps, which both depict numerous areas of severe to extreme drought distributed across this region. A couple of interesting exceptions exist, however; for example, the western portion of ecoregion section 322B-Sonoran Desert and most of section 322C-Colorado Desert display a moisture surplus in the 1-, 3-, and 5-year maps. (The two sections are virtually unforested.)

In addition, the 3- and 5-year *MDZ* maps depict severe to extreme drought conditions along the same section of the Gulf Coast (i.e., in eastern Texas and Louisiana) as highlighted by the 2011 annual map. Because forests in this region may not be as well adapted to drought as those in the Southwest, these conditions might represent a more immediate threat to forest health. In contrast, the drought hot spot observed in the Great Lakes region during 2011 (i.e., in ecoregion section 212L; see fig. 4.2) is small compared with the drought-affected areas depicted in the region by the 3- and 5-year *MDZ* maps. Thus, although drought stress may also be a persistent problem for forests in the Great Lakes region, at least a recent improvement in regional moisture conditions may have positive implications for affected forests.

In some geographic regions, the 5-year *MDZ* map (fig. 4.4) displays more extensive or severe drought conditions than the 3-year *MDZ* map (fig. 4.3). This difference may indicate short-term temporal fluctuations in a long-term pattern of persistent drought for the region of interest, as is the case in the Southwestern United States. It may be explained alternatively by the occurrence of especially intense drought conditions during the early years of the 5-year *MDZ* window (i.e., 2007–08 for the current 2011 analysis). For instance, a part of the Southeastern United States (i.e., in sections 231I-Central Appalachian Piedmont, 232H-Middle Atlantic Coastal Plain and Flatwoods, and 232I-Northern Atlantic Coastal Plain and Flatwoods) exhibits comparatively worse drought conditions in the 5-year *MDZ* map than in the 3-year map; a historically exceptional drought that occurred during 2007 (O'Driscoll 2007) likely explains this discrepancy, as well as a similarly observable difference in central to southern Florida. Thus, while the 1-year, 3-year, and 5-year *MDZ* maps together provide a fairly comprehensive short-term overview, it may also be important to consider a particular region's longer term drought history when assessing the current health of its forests.

Hawaii

With the exception of Kaho'olawe, which is relatively flat, the major islands of Hawaii (fig. 4.5) display rugged topography, often transitioning quickly from coastal lowlands to inland mountains along steep elevation gradients. The largest island, Hawai'i, is dominated by the volcanoes Mauna Kea and Mauna Loa, both of which approach 14,000 feet in elevation; the volcano Haleakala on the island of Maui rises to approximately 10,000 feet. Each of these volcanoes is encircled by a subalpine zone (6,000 to 6,500 feet in elevation) that features certain shrub communities that extend above treeline, which is approximately 8,200 feet (Cordell and others 2000, Cuddihy 1989). A true alpine ecological zone exists only on the high slopes of Mauna Kea and Mauna Loa (Cuddihy 1989).

The major islands of Hawaii all exhibit a similar, concentric pattern of vegetation distribution (Noguchi 1992). A key factor behind this pattern (fig. 4.6) is the influence of northeasterly trade winds, which interact with the islands' mountains to create dramatic variations in precipitation levels (Cuddihy 1989, Noguchi 1992). The winds essentially bring moisture across the windward (i.e., northeastern) sides of the islands; in turn, as elevation increases and air temperature decreases, this moisture is released as rainfall. Due to this effect, some windward locations receive more than 15 times the rainfall observed

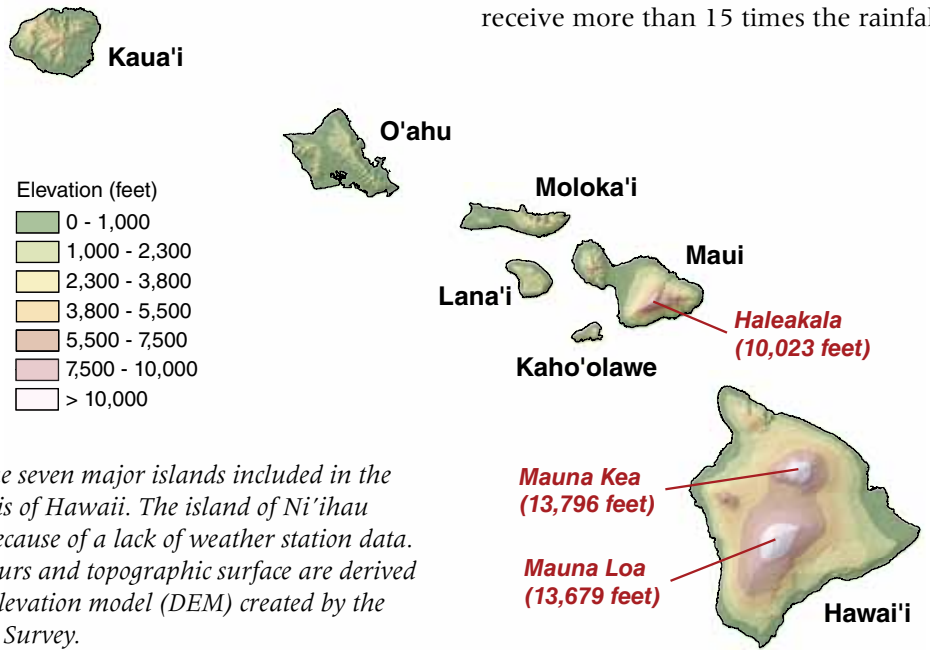

Figure 4.5—The seven major islands included in the drought analysis of Hawaii. The island of Ni'ihau was excluded because of a lack of weather station data. Elevation contours and topographic surface are derived from a digital elevation model (DEM) created by the U.S. Geological Survey.

over the open ocean near Hawaii (Loope and Giambelluca 1998). For instance, the peaks and upper slopes of Kaua'i, O'ahu, and Moloka'i are extremely wet, supporting dense forests. In contrast, leeward (i.e., southwestern) slopes and low-lying areas of the islands, because they are in the rain shadows of the mountains, are typically dominated by grasslands, or, in some cases, woodlands (i.e., tree cover between 10 and 50 percent) and shrublands (Cuddihy 1989). The limited forest cover on Kaho'olawe and Lana'i is likewise explained by the fact that both islands lie in the rain shadow of Maui (Chu and others 2009, Cuddihy 1989). A departure from this general windward-leeward trend is the Kona (i.e., west-southwest) coast of Hawai'i, where a distinctive pattern of onshore sea breezes results in some unique weather behavior; in short, this area is wet enough to support a narrow band of forests near the coastline (Chu and others 2009, Cuddihy 1989). In addition, on Maui and on Hawai'i, a temperature inversion layer between 5,900 and 7,900 feet prevents moisture-laden air masses from rising above this elevation zone (Juvik and Nullet 1994, Noguchi 1992). As a result, the upper slopes of Mauna Kea, Mauna Loa, and Haleakala are extremely dry and nearly devoid of vegetation.

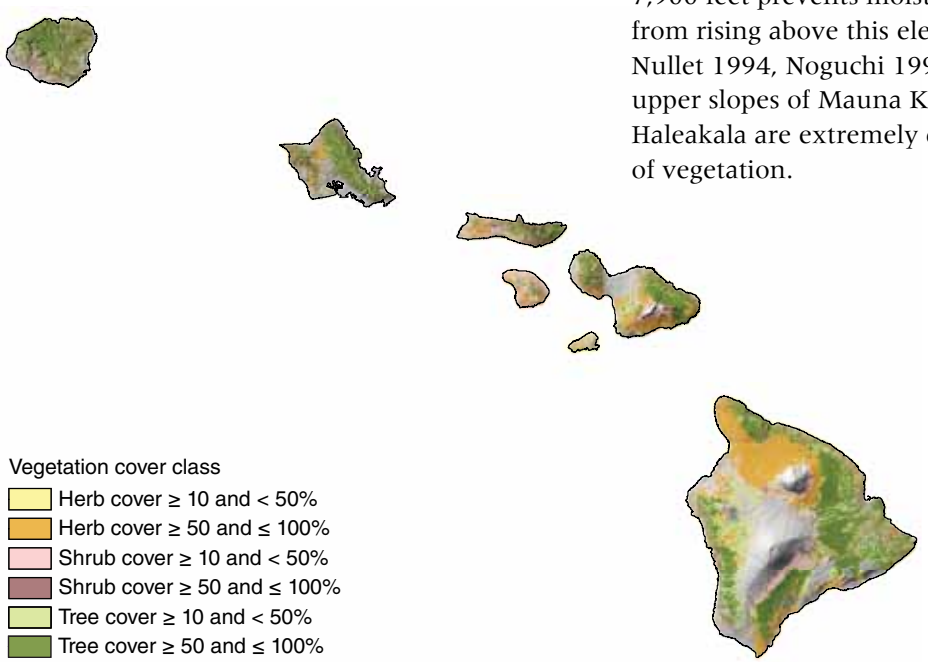

Figure 4.6—The vegetation of Hawaii, categorized according to the percentage cover of the predominant life form (i.e., herb, shrub, or tree). Agricultural, developed, and barren areas have been omitted. Underlying topographic surface is derived from a digital elevation model (DEM) created by the U.S. Geological Survey. (Data source: LANDFIRE.)

The long-term (i.e., 88-year) mean annual moisture index, or $MI_{1\,norm}'$, grid for Hawaii (fig. 4.7) is consistent with the vegetation distribution pattern shown in figure 4.6: the windward slopes of the islands are moderate to very wet ($MI' > 0.3$), while leeward and high-elevation areas—other than Hawai'i's Kona coast—are moderate to extremely dry ($MI' < -0.3$). Most of the areas with dense (≥ 50 percent) tree cover exhibit positive MI' values, although patches of "dry forest" (with negative MI' values) are distributed throughout the islands (Cuddihy 1989). The grid ($MI_{1\,SD}'$) showing the long-term standard deviation of the annual moisture index is not shown; to summarize it briefly, dry leeward areas usually display high levels of variability in the index, while wet windward areas typically display low levels of variability. One exception is a very dry ($MI' < -0.7$) area along the northwestern coast of the island of Hawai'i, which likewise exhibits low variability.

Drought has been a chronic problem for Hawaii (Chu 1989). Significantly, drought conditions in the State appear to be linked to the El Niño-Southern Oscillation (ENSO) cycle, with dry conditions tending to emerge in El

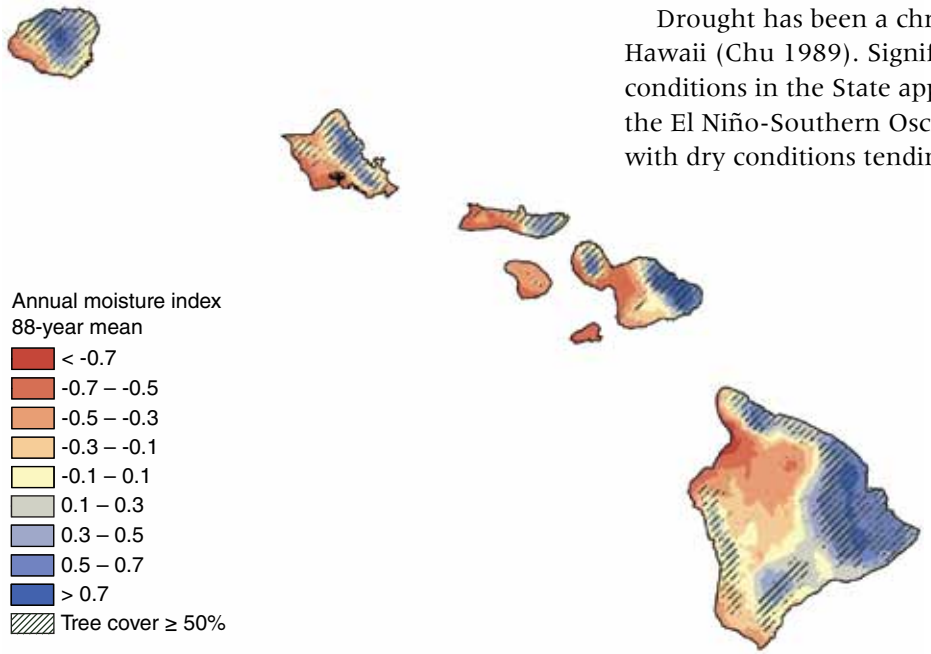

Figure 4.7—The mean annual moisture index, or $\mathrm{MI}_{1}{}'_{\mathrm{norm}}$ *for Hawaii based on 88 years (1920–2007) of available data. To enhance display, the* $\mathrm{MI}_{1}{}'_{\mathrm{norm}}$ *map was resampled to 240-m resolution using the cubic convolution method. Tree cover map (overlaid green hatching) was developed by LANDFIRE (see fig. 4.6). (Data sources: Giambelluca and others 2011, National Climatic Data Center 2012a.)*

Niño years and to last into the immediately following years, while La Niña years typically bring wet conditions (Chu 1989, 1995; Chu and Chen 2005). Furthermore, because the ENSO cycle operates on a fluctuating time scale of 2 to 8 years (Chu and Chen 2005), droughts—and likewise, moisture surpluses—occur rather frequently. On a broader (i.e., interdecadal) time scale, the Pacific Decadal Oscillation (PDO) signal has also shown a negative influence on Hawaiian rainfall. Chu and Chen (2005) described an epoch of low rainfall that lasted from the mid-1970s until 2001 but that came after a similarly long epoch (i.e., almost 28 years) of high rainfall.

A time series of annual (i.e., 1-year) *MDZ* maps (fig. 4.8) depicts the dynamic moisture conditions that occurred in Hawaii between the late 1970s and mid-1980s, i.e., in the early portion of the "dry" epoch reported by Chu and Chen (2005). (The corresponding 3-year and 5-year *MDZ* maps are not shown.) The first map in the series (fig. 4.8A), which depicts conditions during 1979, shows only scattered areas of moderate or worse drought, primarily limited to O'ahu and Kaua'i. Although 1979 is not documented as either an El Niño or La Niña year, the presence of moisture surplus conditions across much of the State may reflect a protracted period of heavy rainfall that occurred in January and February 1979, especially on Hawai'i (Jayawardena and others 2012). In contrast, the 1981 map (fig. 4.8B) shows extensive areas of moderate to extreme drought on Maui and Hawai'i, coinciding with an El Niño event that began in 1980 and continued into the next year (Chu and Chen 2005). The 1983 map (fig. 4.8C) depicts large regions of extreme drought on Hawai'i, O'ahu, and Kaua'i and at least moderate drought conditions across most of the major islands. An exceptionally strong El Niño event, with record-low rainfall, occurred in 1982–83; the severity of the event prompted officials to impose strict water rationing in parts of the State during subsequent years (Chu 1989, Loope and Giambelluca 1998). By 1985, which was a La Niña year (Chu and Chen 2005), most of Hawaii had returned to near normal or surplus moisture conditions, with small pockets of moderate to severe drought appearing on Hawai'i and Kaua'i (fig. 4.8D).

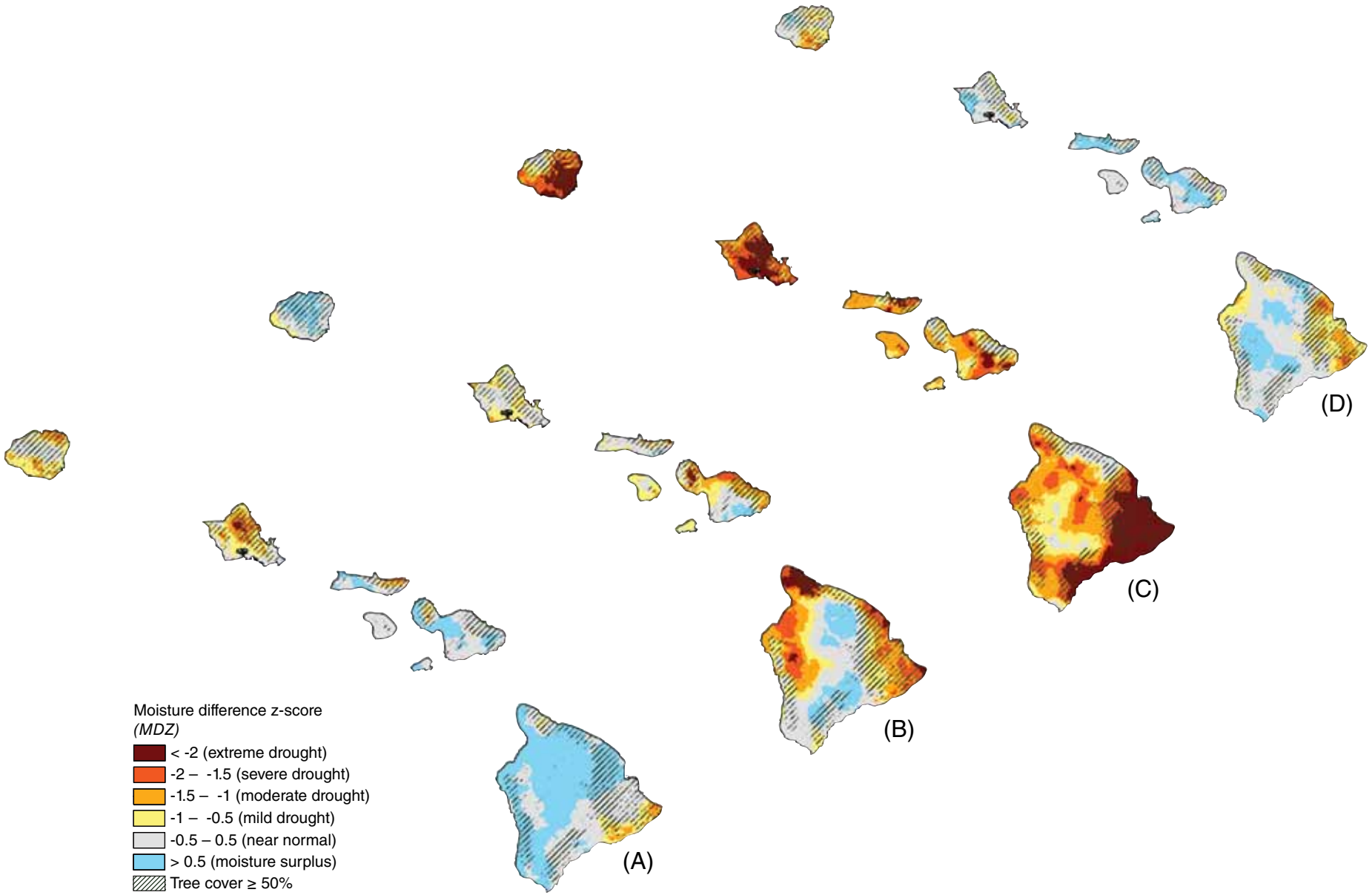

Figure 4.8—Chronological sequence of annual (i.e., 1-year) moisture difference z*-score, or* MDZ*, maps for Hawaii: (A) 1979, (B) 1981, (C) 1983, and (D) 1985. To enhance display, the* MDZ *maps were resampled to 240-m resolution using the cubic convolution method. Tree cover map (overlaid green hatching) was developed by LANDFIRE (see fig. 4.6). (Data sources: Giambelluca and others 2011, National Climatic Data Center 2012a.)*

Because the ENSO and PDO cycles operate at such large geographic scales, one might expect little variation among the individual islands of Hawaii in terms of drought frequency. This is largely affirmed by a set of maps (fig. 4.9) depicting the frequencies at which certain levels of drought intensity (see table 4.1) occur across the State. (The maps depict annual drought frequencies; the 3- and 5-year drought frequency maps have been omitted.) When considered as a group, the maps straightforwardly show that as drought intensity increases, the frequency of occurrence tends to decrease. A more subtle yet still important point is that the range of variation in the frequency values is fairly small within each map. For example, in the map depicting frequency of mild or worse drought conditions (fig. 4.9A), the frequencies are mostly in the 0.20 to 0.40 range, while in the map depicting the frequency of moderate or worse drought conditions (fig. 4.9B), they are in the 0.10 to 0.25 range. Furthermore, in the map depicting the frequency of extreme drought (fig. 4.9D), the frequencies are rarely above 0.05. Nevertheless, an interesting pattern emerges despite the limited variability. In figure 4.9A, and figure 4.9B to a lesser degree, there appears to be a slightly higher frequency of drought conditions on the leeward side of most islands, which is to be expected given the importance of the trade winds to the overall moisture regime. In the map depicting the frequency of at least severe drought conditions (fig. 4.9C), however, this pattern is reversed: the frequencies tend to be slightly higher on the windward sides of the islands or, more simply, in areas that are normally wet (see fig. 4.7). To some extent, figure 4.9D also displays this pattern. This apparent switch in the frequency pattern probably relates to our depiction of drought as a standardized departure from normal conditions. In equation 3, a map cell's MDZ_{ij} value depends on the cell's long-term normal moisture index (MI'_{norm}) value and its standard deviation (MI'_{SD}). Under this approach, locations where the amount of moisture is stable through time (i.e., areas with low MI'_{SD}) are more sensitive to small departures from average conditions, such that a small negative difference between the MI'_{norm} (i.e., the long-term normal) value and the MI' value for a particular year of interest can translate to a relatively low MDZ value for that year. In the case of Hawaii, these low-variability areas tend to be wetter. Conversely, areas where the amount of moisture is highly variable through time (i.e., areas with high MI'_{SD}) are far less sensitive, so it may require a relatively large difference between MI'_{norm} and the MI' value for the target year to achieve a low MDZ value. In Hawaii, these high-variability areas are often drier. This suggests that, ultimately, it is important to consider the long-term moisture regime (fig. 4.7) when assessing the impact of reported drought conditions in particular areas of Hawaii.

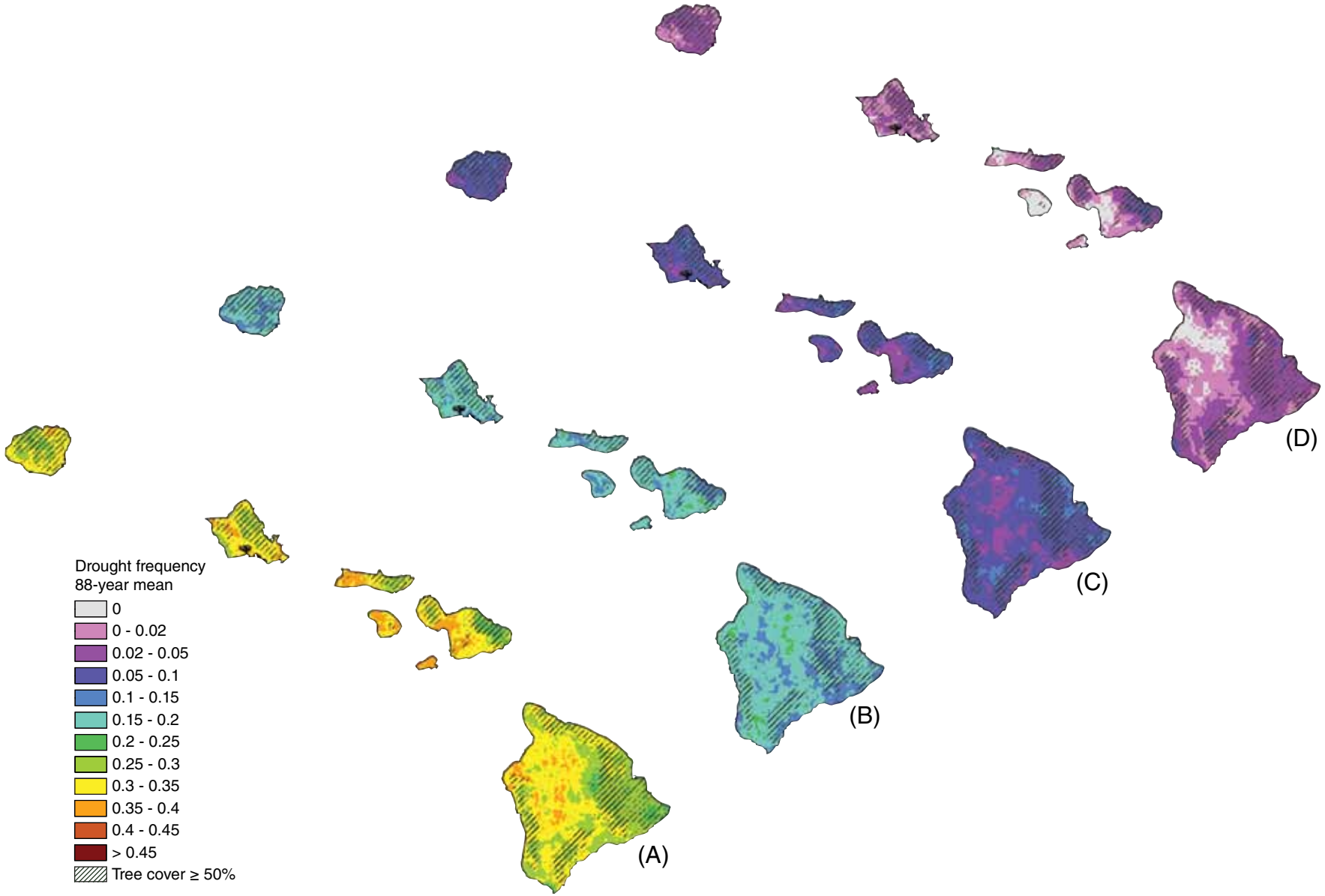

*Figure 4.9—One-year drought frequency maps for Hawaii: frequency of (A) at least mild drought (*MDZ < -0.5*), (B) at least moderate drought (*MDZ < -1*), (C) at least severe drought (*MDZ < -1.5*), and (D) extreme drought (*MDZ < -2*). To enhance display, the frequency maps were resampled to 240-m resolution using the cubic convolution method. Tree cover map (overlaid green hatching) was developed by LANDFIRE (see fig. 4.6). (Data sources: Giambelluca and others 2011, National Climatic Data Center 2012a.)*

Future efforts

If the appropriate spatial data (i.e., high-resolution maps of precipitation and temperature) continue to be available for public use, we expect to produce our 1-, 3-, and 5-year *MDZ* maps of the conterminous United States as a regular yearly component of national-scale forest health reporting. Unfortunately, a similar goal for the State of Hawaii is probably impractical given the potential lack of contemporary weather data and the need to create our own gridded datasets via spatial interpolation. Nevertheless, we anticipate returning to the topic of drought in Hawaii at some point in time. One particular aspect that may be worth further investigation is our choice of spatial interpolation method; for example, we may want to compare datasets generated via cokriging with results from other interpolation methods that do not employ semivariogram estimation. In any case, it is important for users to interpret and compare the *MDZ* drought maps presented here cautiously. Although the maps use a standardized index scale that applies regardless of the size of the time window, it should also be understood that, for instance, an extreme drought that persists over a 5-year period has substantially different forest health implications than an extreme drought over a 1-year period. In future work, we hope to provide forest managers and other decisionmakers with better quantitative evidence regarding some of these relationships between drought and forest health.

LITERATURE CITED

Akin, W.E. 1991. Global patterns: climate, vegetation, and soils. Norman, OK: University of Oklahoma Press. 370 p.

Archaux, F.; Wolters, V. 2006. Impact of summer drought on forest biodiversity: what do we know? Annals of Forest Science. 63: 645-652.

Chu, P.-S. 1989. Hawaiian drought and the Southern Oscillation. International Journal of Climatology. 9: 619-631.

Chu, P.-S. 1995. Hawaii rainfall anomalies and El Niño. Journal of Climate. 8: 1697-1703.

Chu, P.-S.; Chen, H. 2005. Interannual and interdecadal rainfall variations in the Hawaiian Islands. Journal of Climate. 18: 4796-4813.

Chu, P.-S.; Zhao, X.; Ruan, Y.; Grubbs, M. 2009. Extreme rainfall events in the Hawaiian Islands. Journal of Applied Meteorology and Climatology. 48: 502-516.

Clark, J.S. 1989. Effects of long-term water balances on fire regime, north-western Minnesota. Journal of Ecology. 77: 989-1004.

Cleland, D.T.; Freeouf, J.A.; Keys, J.E., Jr. [and others]. 2007. Ecological subregions: sections and subsections for the conterminous United States. 1:3,500,000; Albers equal area projection; colored. In: Sloan, A.M., tech. ed. Gen. Tech. Rep. WO-76. Washington, DC: U.S. Department of Agriculture Forest Service. Also as a GIS coverage in ArcINFO format on CD-ROM or at http://fsgeodata.fs.fed.us/other_resources/ecosubregions.html. [Date accessed: May 9, 2011].

Clinton, B.D.; Boring, L.R.; Swank, W.T. 1993. Canopy gap characteristics and drought influences in oak forests of the Coweeta Basin. Ecology. 74(5): 1551-1558.

Cordell, S.; Goldstein, G.; Melcher, P.J.; Meinzer, F.C. 2000. Photosynthesis and freezing avoidance in ohia (*Metrosideros polymorpha*) at treeline in Hawaii. Arctic, Antarctic, and Alpine Research. 32(4): 381-387.

Cressie, N.A.C. 1993. Statistics for spatial data. New York: John Wiley & Sons. 900 p.

Cuddihy, L.W. 1989. Vegetation zones of the Hawaiian Islands. In: Stone, C.P.; Stone, D.B., eds. Conservation biology in Hawaii. Honolulu: University of Hawaii Press: 27-37.

Daly, C.; Gibson, W.P.; Taylor, G.H. [and others]. 2002. A knowledge-based approach to the statistical mapping of climate. Climate Research. 22: 99-113.

ESRI. 2010. ArcGIS. Version 10.0. Redlands, CA: Environmental Systems Research Institute.

Giambelluca, T.W.; Chen, Q.; Frazier, A.G. [and others]. 2011. The rainfall atlas of Hawai'i. http://rainfall.geography.hawaii.edu. [Date accessed: January 17, 2012].

Goovaerts, P. 1998. Ordinary cokriging revisited. Mathematical Geology. 30(1): 21-41.

Goovaerts, P. 2000. Geostatistical approaches for incorporating elevation into the spatial interpolation of rainfall. Journal of Hydrology. 228: 113-129.

Gómez, J. D.; Etchevers, J.D.; Monterroso, A.I. [and others]. 2008. Spatial estimation of mean temperature and precipitation in areas of scarce meteorological information. Atmósfera 21:35-56.

Groisman, P.Y.; Knight, R.W. 2008. Prolonged dry episodes over the conterminous United States: new tendencies emerging during the last 40 years. Journal of Climate. 21: 1850-1862.

Guarín, A.; Taylor, A.H. 2005. Drought triggered tree mortality in mixed conifer forests in Yosemite National Park, California, USA. Forest Ecology and Management. 218: 229-244.

Hanson, P.J.; Weltzin, J.F. 2000. Drought disturbance from climate change: response of United States forests. The Science of the Total Environment. 262: 205-220.

Hevesi, J.A.; Istok, J.D.; Flint, A.L. 1992. Precipitation in mountainous terrain using multivariate geostatistics. Part I: structural analysis. Journal of Applied Meteorology. 31: 661-676.

Hinckley, T.M.; Dougherty, P.M.; Lassoie, J.P. [and others]. 1979. A severe drought: impact on tree growth, phenology, net photosynthetic rate, and water relations. American Midland Naturalist. 102(2): 307-316.

Ishida, T.; Kawashima, S. 1993. Use of cokriging to estimate surface air temperature from elevation. Theoretical and Applied Climatology. 47: 147-157.

Jayawardena, I.M.S.; Chen, Y.-L.; Nash, A.J.; Kodama, K. 2012. A comparison of three prolonged periods of heavy rainfall over the Hawaiian Islands. Journal of Applied Meteorology and Climatology. 51: 722-744.

Johnston, K.; Ver Hoef, J.M.; Krivoruchko, K.; Lucas, N. 2003. Using ArcGIS geostatistical analyst. Redlands, CA: Environmental Systems Research Institute. 300 p.

Juvik, J.O.; Nullet, D. 1994. A climate transect through tropical montane rain forest in Hawaii. Journal of Applied Meteorology. 33: 1304-1312.

Kareiva, P. M.; Kingsolver, J.G.; Huey, B.B, eds. 1993. Biotic interactions and global change. Sinauer Associates, Inc., Sunderland, MA. 559 p.

Keetch, J.J.; Byram, G.M. 1968. A drought index for forest fire control. Res. Pap. SE-38. Asheville, NC: U.S. Department of Agriculture Forest Service, Southeastern Forest Experiment Station. 33 p.

Koch, F.H.; Coulston, J.W.; Smith, W.D. 2012a. High-resolution mapping of drought conditions. In: Potter, K.M.; Conkling, B.L., eds. Forest health monitoring 2008 national technical report. Gen. Tech, Rep. SRS-158. Asheville, NC: U.S. Department of Agriculture Forest Service, Southern Research Station: 45-62.

Koch, F.H.; Coulston, J.W.; Smith, W.D. 2012b. Mapping drought conditions using multi-year windows. In: Potter, K.M.; Conkling, B.L., eds. Forest health monitoring 2009 national technical report. Gen. Tech. Rep. SRS-167. Asheville, NC: U.S. Department of Agriculture Forest Service, Southern Research Station: 163-178. Chapter 10.

Koch, F.H.; Smith, W.D.; Coulston, J.W. 2013a. An improved method for standardized mapping of drought conditions. In: Potter, K.M.; Conkling, B.L., eds. Forest health monitoring: national status, trends, and analysis 2010. Gen. Tech. Rep. SRS-176. Asheville, NC: U.S. Department of Agriculture Forest Service, Southern Research Station: 67-82. Chapter 6.

Koch, F.H.; Smith, W.D.; Coulston, J.W. 2013b. Recent drought conditions in the conterminous United States. In: Potter, K.M.; Conkling, B.L., eds. Forest health monitoring: national status, trends, and analysis 2011. Gen. Tech. Rep. SRS-185. Asheville, NC: U.S. Department of Agriculture Forest Service, Southern Research Station: 41-56. Chapter 4.

Loope, L.L.; Giambelluca, T.W. 1998. Vulnerability of island tropical montane cloud forests to climate change, with special reference to East Maui, Hawaii. Climatic Change. 39: 503-517.

Mattson, W.J.; Haack, R.A. 1987. The role of drought in outbreaks of plant-eating insects. BioScience. 37(2): 110-118.

McDowell, N.; Pockman, W.T.; Allen, C.D. [and others]. 2008. Mechanisms of plant survival and mortality during drought: why do some plants survive while others succumb to drought? New Phytologist. 178: 719-739.

Millar, C.I.; Westfall, R.D.; Delany, D.L. 2007. Response of high-elevation limber pine (*Pinus flexilis*) to multiyear droughts and 20th-century warming, Sierra Nevada, California, USA. Canadian Journal of Forest Research. 37: 2508-2520.

Mueller, R.C.; Scudder, C.M.; Porter, M.E. [and others]. 2005. Differential tree mortality in response to severe drought: evidence for long-term vegetation shifts. Journal of Ecology. 93: 1085-1093.

National Climatic Data Center. 2007. Time bias corrected divisional temperature-precipitation-drought index. Documentation for dataset TD-9640. http://www1.ncdc.noaa.gov/pub/data/cirs/drought.README. [Date accessed: July 20, 2010].

National Climatic Data Center. 2010. State of the climate—drought—annual report 2009. http://www.ncdc.noaa.gov/sotc/2009/13. [Date accessed: May 12, 2011].

National Climatic Data Center. 2011. State of the climate—drought—annual report 2010. http://www.ncdc.noaa.gov/sotc/drought/2010/13. [Date accessed: May 10].

National Climatic Data Center. 2012a. Climate data online—monthly surface data (DS3220). http://cdo.ncdc.noaa/pls/plclimprod/somdmain. somdwrapper?datasetabbv=DS3220& countryabbv=&georegionabbv=&forceoutside=. [Date accessed: February 17].

National Climatic Data Center. 2012b. State of the climate—drought—annual report 2011. http://www.ncdc.noaa.gov/sotc/drought/2011/13. [Date accessed: April 26].

Noguchi, Y. 1992. Vegetation asymmetry in Hawaii under the trade wind regime. Journal of Vegetation Science. 3: 223-230.

O'Driscoll, P. 2007. A drought for the ages: from the dried lake beds of Florida to the struggling ranches of California, a historic lack of rain is changing how Americans live. USA Today. June 8: 1A.

Palmer, W.C. 1965. Metereological drought. Res. Pap. No. 45. Washington, DC: U.S. Department of Commerce, Weather Bureau. 58 p.

Phillips, D.L.; Dolph, J.; Marks, D. 1992. A comparison of statistical procedures for spatial analysis of precipitation in mountainous terrain. Agricultural and Forest Meteorology. 58: 119-141.

PRISM Group. 2012. 2.5-arcmin (4 km) gridded monthly climate data. ftp://prism.oregonstate.edu//pub/prism/us/grids. [Date accessed: April 23, 2012].

Schoennagel, T.; Veblen, T.T.; Romme, W.H. 2004. The interaction of fire, fuels, and climate across Rocky Mountain forests. BioScience. 54(7): 661-676.

Svoboda, M.; LeComte, D.; Hayes, M. [and others]. 2002. The drought monitor. Bulletin of the American Meteorological Society. 83(8): 1181-1190.

Thornthwaite, C.W. 1948. An approach towards a rational classification of climate. Geographical Review. 38(1): 55-94.

Willmott, C.J.; Feddema, J.J. 1992. A more rational climatic moisture index. Professional Geographer. 44(1): 84-87.